Load-deformation behaviour of concrete tension ties with weft-knitted textile reinforcement

Author(s):
Lee, Minu; Mata Falcón, Jaime; Kaufmann, Walter

Publication date:
2020-08

Permanent link:
https://doi.org/10.3929/ethz-b-000438439

Load-Deformation Behaviour of Concrete Tension Ties with Weft-Knitted Textile Reinforcement

Minu Lee, Jaime Mata-Falcón and Walter Kaufmann

Institute of Structural Engineering (IBK),
Swiss Federal Institute of Technology Zurich (ETHZ),
Stefano-Franscini-Platz 5, 8093 Zurich, Switzerland

Abstract
The use of non-corrosive high-strength fibrous materials as textile reinforcement allows the construction of more slender elements when compared to members with conventional steel reinforcing bars. This paper explores the load-deformation behaviour of weft-knitted textile reinforcement embedded in a fine grain concrete. In this experimental study, flat concrete specimens with a thickness of 12-16 mm are loaded in uniaxial tension. The study focuses on the comparison of various knitting patterns, materials and geometric features in the knitted textile. Results show that the post-cracking behaviour can be improved for certain configurations in terms of ultimate strength and deformation capacity. The failure mode is governed by the material of the fibres and their coating.

1 Introduction

Textile reinforcement is made from high-strength continuous fibres, which exist in a wide variety from synthetic polymers such as aramid or carbon fibres to inorganic materials such as glass fibre [1], that form rovings, i.e., bundles of thicker strands. Usually, these rovings are coated or fully impregnated with a resin (e.g. epoxy) to improve their resistance against abrasion and the inter-fibre friction, thereby enhancing the stress transfer and distribution within the strand of multiple filaments and hence, increasing the roving's strength [2]. The majority of existing literature covers flat sheets from orthogonally woven grids of straight rovings (e.g. [3], [4]), but little attention has been given to weft-knitted textiles, which have a great advantage in their geometric definition: They allow for complex shapes without the need of stitching multiple patches together [5]. CNC knitting machines allow to locally vary the length and width of the textile by adding or omitting loops and to include spatial features such as channels or ribs [6]. The KnitCrete technology developed at ETH Zürich [7] uses a weft-knitted textile as stay-in-place formwork. The textile is tensioned in a scaffolding frame and it is initially coated with a thin layer of fast-setting cement paste. After hardening, this first layer serves as a stable and stiff formwork for the subsequent application of concrete. The technology was successfully applied in the construction of the KnitCandela pavilion, which was collaboratively realised by Block Research Group (ETHZ) and Zaha Hadid Architects in Mexico City [8]. However, the approach did not explicitely address the integration of reinforcement within the fabrication procedure. Possibilities arising from knitting are summarised in [6]. A potential solution is the activation of the weft-knitted textile as reinforcement – rather than just as lost formwork – by utilising high-strength fibrous materials. Special care needs to be given to the interface between coated textile and the concrete to ensure proper stress transfer. This paper presents an experimental study consisting of uniaxial tension tests on flat concrete sheets with one centred layer of coated textile reinforcement (Fig. 1). The investigations focus on various knitting patterns, types of fibres and coating as well as spatial features within the textiles to enhance the bond between reinforcement and concrete.

2 Experimental campaign

This section summarises the materials, the preparation of the specimens and the test setup including the test protocol and measurement devices.

2.1 Materials, specimens and production

Fibres made of three different materials were used for the textile reinforcement: aramid (AR), carbon fibre (CF) and E-glass (GF), which all have a high tensile strength and adequate to high elasticity modulus, but are sensitive to lateral loading. The notional material properties are shown in Table 1.

Table 1 Properties of textile rovings.

Material	$f_{t,u}$	E_t	ρ_t
	[MPa]	[GPa]	[g/cm^3]
Aramid	3'000	100	1.44
Carbon fibre	4'300	240	1.76
Glass fibre	2'700	73	2.55

Two different types of coating were examined: a highly fluid cement paste consisting of a blended ordinary Portland cement, a polycarboxylate ether based superplasticiser and stabilising nanoparticles [7] (mix design courtesy of Chair of Physical Chemistry of Building Materials at ETH Zürich), and furthermore, a low-viscous two-component epoxy suitable for hand lamination of textile fibres.

The coated textiles were embedded in a fine grain concrete with a maximum aggregate size of D_{max} = 2 mm and a *w*/*c*-ratio of 0.4, which was mixed in the laboratory (Fig. 1c). The flexural tensile strength was obtained from small prisms (40 mm×40 mm×160 mm) according to EN 196-1 [9]. The material tests for the different batches were conducted at 8 and 13 days after casting, without a significant difference. The uniaxial tensile strength was calculated using Eq. (1) taken from fib Model Code [10]. Considering the depth of the prism h_b = 40 mm, the mean flexural tensile strength of 9.5 MPa results in a uniaxial tensile strength of 4.2 MPa.

$$f_{ctm} = \alpha_{fl} \cdot f_{ctm,fl} \qquad \text{where} \qquad \alpha_{fl} = \frac{0.06 \cdot h_b^{0.7}}{1 + 0.06 \cdot h_b^{0.7}} \tag{1}$$

A total of 28 specimens – with dimensions of 200 mm width, 800 mm height and thicknesses between 12 and 16 mm – were manufactured and tested to failure. The textile reinforcement was produced in a CNC knitting machine (Steiger Libra 3.130) and then tensioned in a wooden frame by hand (Fig. 1a). The pre-stress mostly serves to reduce deflections during application of the coating and has no significant relevance for the mechanical behaviour since the forces are very low when compared to the tensile strength of the yarn. The fabrics were coated and left for 3 days to harden in a climate chamber at 20°C and 90% relative humidity in case of cement paste (Fig. 1b) and one day at room temperature in case of epoxy. The coated textile was cut according to the specimen size, embedded onto a first layer of concrete with a thickness of 5 mm, and finally sealed with another top layer of 5 mm concrete cover (Fig. 1c). The concrete was vibrated on a shaking table during the placing of the reinforcement to minimise air voids. The specimens were put in the climate chamber to harden for at least 8 days.

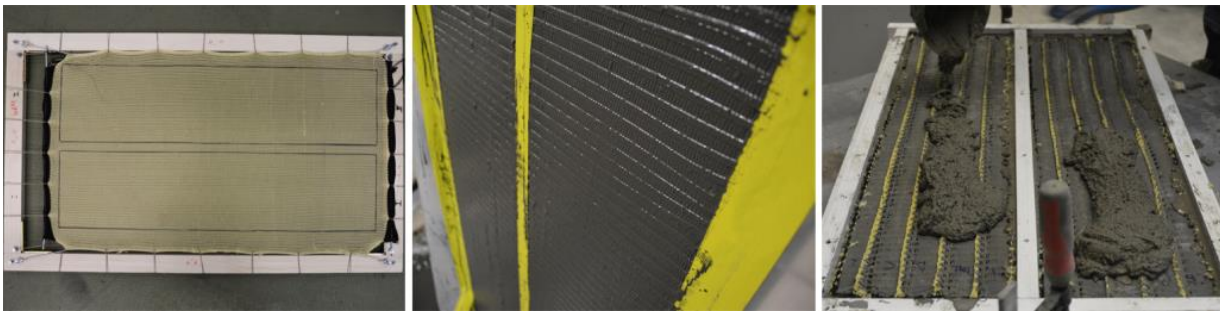

(a) (b) (c)

Fig. 1 Production of specimens: (a) tensioning and (b) cement paste coating of textile; (c) casting of concrete.

A double bed knitting machine allows for an almost infinite range of possibilities [5] depending on the sequence of activated needles which form the loop in the textile. Fig. 2 shows an overview of different typical knitting patterns and their schematic formation in the double needle bed. The first two patterns in Fig. 2a and Fig. 2b show a single layer fabric that alternates between the needle beds. The interlocked textile in Fig. 2c is a double-layer textile that is formed by mirroring the activated needles with every new row. Those knitting patterns could only be made from aramid with relatively thin yarns (160 tex; 1 tex corresponds to 1 g per meter of yarn) since the knitting needles cannot grab thicker yarns, and carbon or glass fibre yarns do not allow for such small bending radii and would break during fabrication.

In the following, those textiles will be referred to as 'directly knitted reinforcement'. Furthermore, the knitting machine allows for the integration of straight rovings (called inlays) within the knitted textile (white yarns in Fig. 2d), which enables the use of thicker yarns and more brittle materials. In this case, the base knitted textile was made from a non-structural acrylic yarns as it served only as a holder for the straight high-strength rovings.

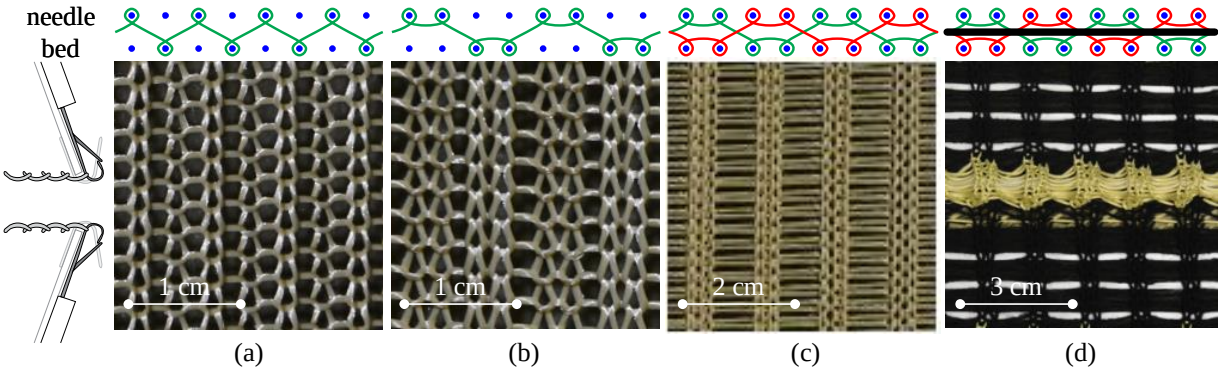

Fig. 2 Knitting patterns: single-layers (a) 1-1 and (b) 2-2; double-layer (c) interlock; (d) interlock with inlays and ribbed texture.

Table 2 Configurations, dimensions and reinforcement content of tested tension ties.

Pattern	Direction	Texture	Fibres & fineness	Coating	#	b [mm]	t [mm]	A_c [mm^2]	A_t [mm^2]
1-1	Warp	Flat	Aramid 160 tex	Cement paste	1	200.7	11.8	2368	12.2
					2	200.0	13.0	2600	11.8
	Weft				1	200.0	12.2	2440	8.2
					2	200.8	13.3	2671	7.9
2-2	Warp	Flat	Aramid 160 tex	Cement paste	1	200.3	12.1	2424	14.4
					2	200.7	12.2	2449	13.3
	Weft				1	200.3	11.7	2344	8.6
					2	200.3	11.6	2323	8.7
Inter	Warp	Flat	Aramid 160 tex	Cement paste	1	201.0	15.0	3015	16.0
					2	200.3	14.3	2864	15.1
	Weft				1	201.0	14.0	2814	19.1
					2	200.7	13.9	2790	18.9
	Warp	Ribs	Aramid 160 tex	Cement paste	1	200.3	17.3	3465	16.0
					2	200.7	15.7	3151	16.0
	Weft				1	201.0	15.8	3176	13.3
					2	201.2	14.2	2857	13.3
Inlay	Weft	Ribs	Aramid 800 tex	Cement paste	1	200.7	13.4	2689	15.6
					2	200.8	12.6	2530	15.6
				Epoxy	1	199.8	13.8	2757	15.6
					2	200.0	15.0	3000	15.6
			Carbon fibre 800 tex	Cement paste	1	200.2	13.7	2743	12.7
					2	201.0	13.9	2794	12.7
				Epoxy	1	199.8	14.6	2917	12.7
					2	200.0	14.4	2880	12.7
			Glass fibre 2400 tex	Cement paste	1	200.5	13.8	2767	16.9
					2	201.6	14.1	2843	16.9
				Epoxy	1	200.7	14.7	2950	16.9
					2	200.3	13.5	2704	16.9

The coated textile forms a flat surface that might act as a cold joint over its whole area. Therefore, ribs – that are formed by folding and closing the textile as shown in Fig. 2d – were introduced in some configurations as spatial features to enhance bond conditions between the textile reinforcement and the concrete. A thin aramid yarn with a fineness of 160 tex was used for the ribs. Cement paste coating was applied in all specimens with the thinner aramid yarns whereas for the specimens with inlays, both cement paste and epoxy coating were examined. The directly knitted textile reinforcement was tested in parallel and orthogonally to the knitting direction (called weft and warp) whereas the textiles with inlays were only loaded in weft direction (although it is technically possible to include inlays in warp direction, the structural outcome is the same since both orthogonal directions in woven textiles are independent of each other). The configurations of all specimens (with a repetition of 2), their dimensions and their reinforcement contents are summarised in Table 2.

2.2 Test setup and protocol

The test setup is based on the recommendation of RILEM TC 232-TDT [11]. The specimens were clamped with stiffened plates over a length of 150 mm with a layer of neoprene with a thickness of 2 mm in between, resulting in a free length of 500 mm (Fig. 3). The plates were connected to the testing machine via threaded rods with spherical bearings on either side to create hinged-hinged boundary conditions, which minimises eccentricities in the load introduction. The specimens were loaded in displacement control. The speed was adjusted during the test according to the following scheme:

- Pre-cracking 0.15 mm/min
- During crack formation 0.5 mm/min
- After full crack formation 1.0 mm/min

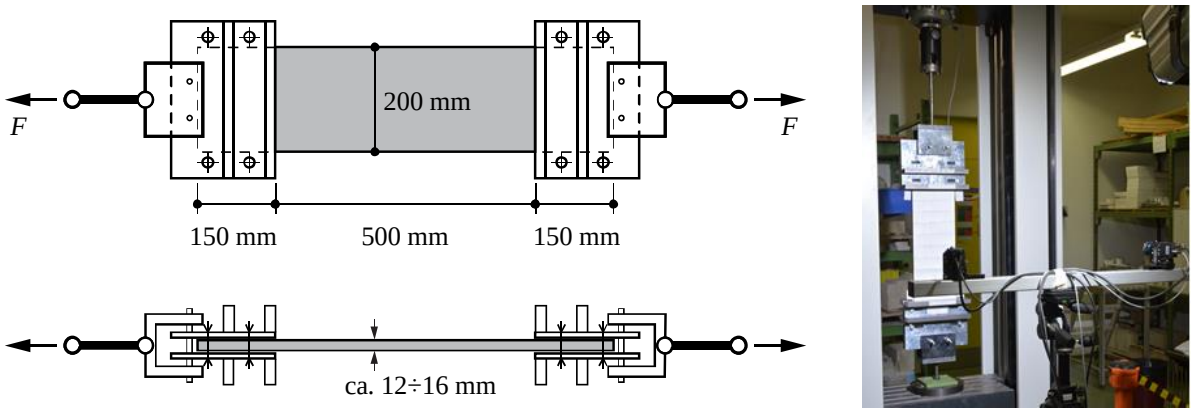

Fig. 3 Test setup (based on the recommendation of RILEM TC 232-TDT): (a) Schematic illustration and dimensions; (b) installed specimen and setup for DIC measurement.

A three dimensional digital image correlation measurement system was used to assess the actual deformations of the specimens and to further investigate the crack kinematics. Therefore, a speckle pattern was applied on one side of the specimen. VIC-3D software by Correlated Solutions was used for the correlation of the results. Small plates with a printed speckle pattern were attached directly onto the specimen in the clamped area to mitigate the effect of slip and deformation of the neoprene in the measurement of the overall elongation.

3 Results and discussion

Basic results of the experimental campaign are presented in the following. Fig. 4 shows the stresses in the textile reinforcement against the mean strains of all specimens where the reinforcement consists of the directly knitted yarn, whereas Fig. 5 summarises all specimens with straight inlays. The nominal textile stresses (σ_t) were calculated by dividing the force from the load cell by the textile cross section. The mean strains (ε_{tm}) were obtained from the total elongation divided by the free length of 500 mm.

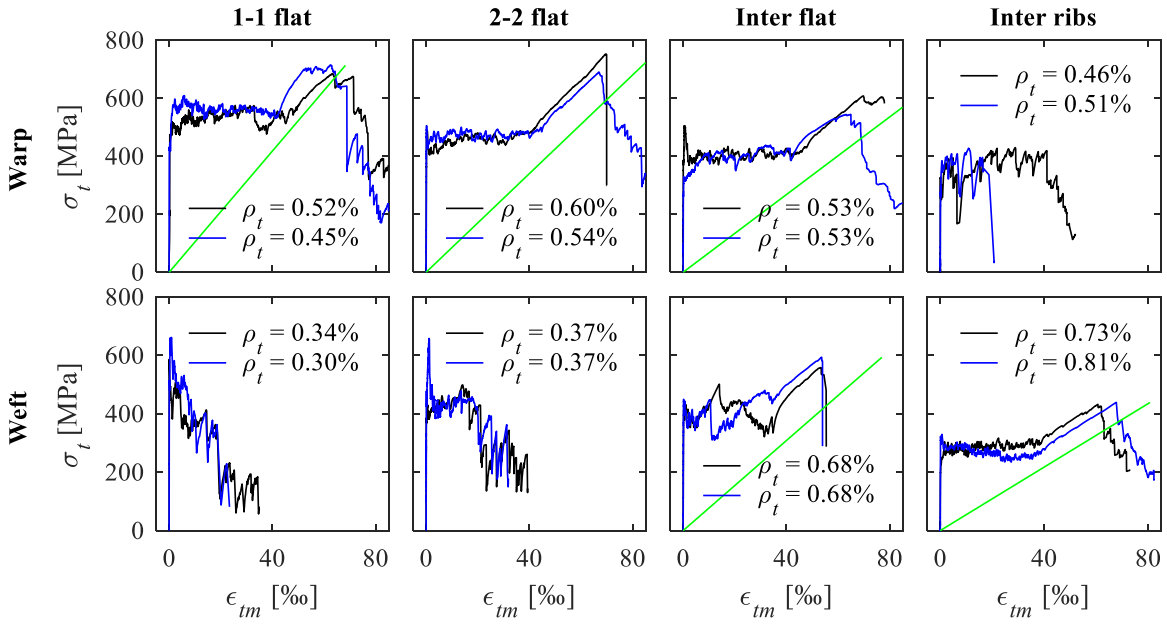

Fig. 4 Textile stress-mean strain-relationship of specimens with directly knitted reinforcement.

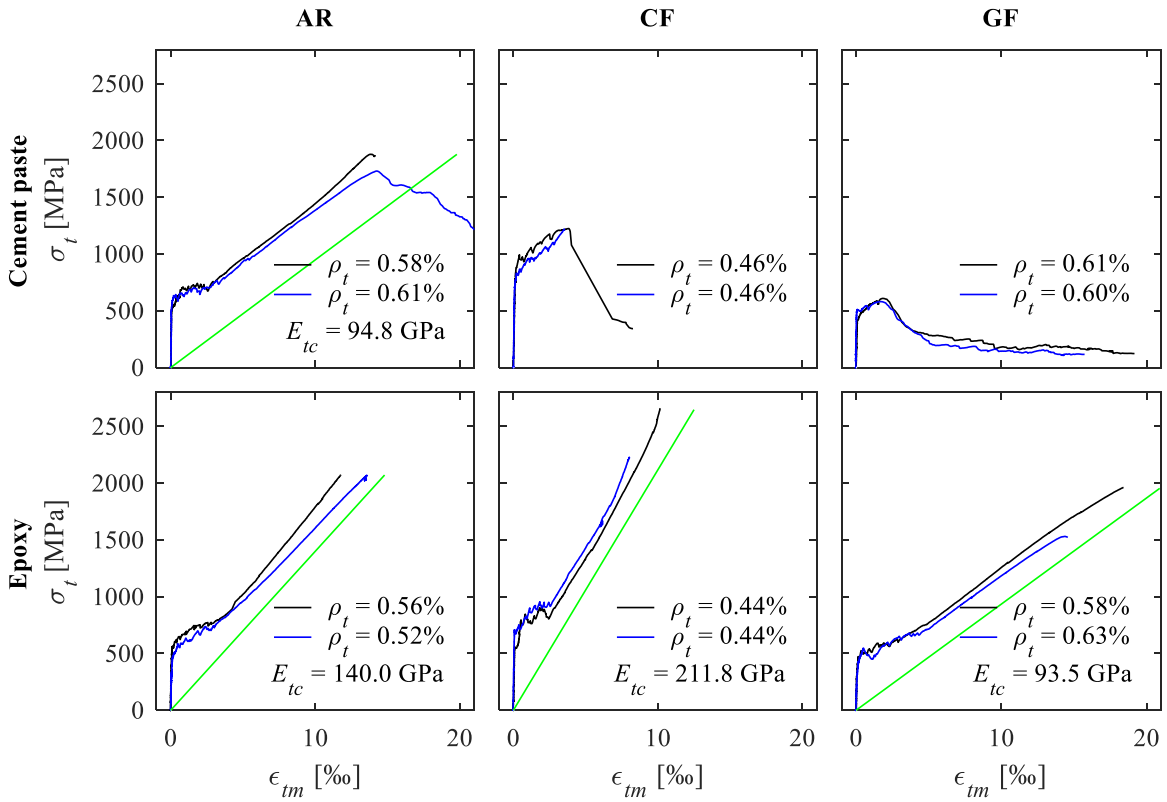

Fig. 5 Textile stress-mean strain-relationship of specimens with straight inlay reinforcement.

3.1 General load-deformation behaviour in pre- and post-cracking phase

Two different types of post-cracking behaviour were observed. Most specimens displayed stable multiple cracking and strain hardening once all cracks are formed. The crack spacing was between 10 mm and 20 mm (determined from visual inspection). However, in some specimens with directly knitted reinforcement (such as the flat interlock pattern and interlock with ribs, both loaded in weft direction), the load decreased right after initial crack formation. This phenomenon has already been observed in strain hardening cementitious composites and potential causes were addressed by Yu et al. [12]. In the present tests, eccentricities caused in the manufacturing of the specimens and in the preparation of the test setup may cause rotations and thus, bending out-of-plane.

In most cases, the failure mode was brittle with a sudden steep drop of textile stresses after reaching the peak load. A progressive failure followed once the tensile strength had been reached in one fibre since the material exhibits no ductility and thus, the stresses cannot be redistributed within the reinforcement. However, in deformation controlled tests, the subsequent failure of individual yarns can cause a softening behaviour, which was mostly observed in the directly knitted reinforcement since the yarn rupture caused a local opening of the interlocked loops (as shown in Fig. 6a), but the remaining textile is able to carry some residual stresses. Spalling of the concrete occured with increasing deformation in the post-peak phase since the textile-concrete interface started to debond and the lateral contraction of the textile initiated buckling of the cover at the edges of the flat tension tie. The integration of ribs in the knitted fabric creates a mechanical connection between the textile and the cover concrete, which hindered spalling.

Some specimens did not display stable cracking and failed directly or shortly after the initial crack had formed. They normally exhibited a softening behaviour, which in case of the straight inlays, seemed to be caused by a pull-out of the fibres rather than progressive failure of the yarns as explained above. From visual inspection, it appears that only the outer fibres of the rovings were ruptured and the inner core was pulled out (Fig. 6b). This failure mode has also been observed in commercially available woven textile reinforcement [4] and is caused by insufficient internal friction of the filaments within the roving.

(a) (b) (c)

Fig. 6 Failure modes: (a) Subsequent failure of interlocked loops and spalling of cover concrete; (b) rupture of outer fibres and pull-out of inner core; (c) full rupture of fibres.

3.2 Strength and utilisation

The utilisation is defined as the maximum nominal tensile stress in the textile divided by the notional tensile strength adopted from the material documentation. The directly knitted textiles displayed low degrees of utilisation. The single-layer knitting patterns (1-1 and 2-2) showed utilisation ratios of around 24% whereas the interlocked double-layer textiles only reached utilisation between 14% and 17%. Therefore, specimens with low reinforcement content already failed upon cracking. The interlocked loops within the knitted textiles leads to small bending radii (with 180°-bents) and to concentrated introduction of lateral forces at the bends of the yarn, which explains the observed significant reduction in strength. The interlocked double-layer knitting pattern exhibits a much denser structure and the integration of ribs creates additional weakening impairing the utilisation.

The specimens with straight inlays performed much better (utilisation between 50% and 70%) since the rovings are only loaded in their axial direction. The contribution of the aramid fibres in the ribs was neglected in the determination of the utilisation since they exhibit much lower stiffness than the straight rovings and, therefore, do not get significantly activated. Eventually, the nominal textile stresses do not reach the full notional tensile strength due to several reasons: (i) Stresses spread across the cross section of a roving via internal friction between individual filaments, which depends on the type of coating and the depth of penetration into the roving [4]. The core fibres might not be loaded yet while the outer fibres of the roving already reach the tensile strength. (ii) Eccentricities in the specimen and in the test setup may cause a deviation of the roving at the crack edges and, therefore, damage the yarn and introduce highly concentrated lateral forces on the reinforcement [3]. (iii) The brittle nature of the fibre material prevents a redistribution of stresses after the first fibre breaks, which makes it more prone to premature failure due to local material deficiencies. A suitable coating or impregnation of the yarns can reduce or even mitigate those effects, whereas in the comparison of cement paste and epoxy, the latter had a more beneficial influence. The specimens with carbon and glass fibre inlays coated with cement paste failed shortly after initial cracking. These fibres are more sensitive to lateral loading than aramid

and can be easily broken even by hand when sharply folded. However, their epoxy-coated counterparts showed much higher failure loads with clean rupture of all rovings (Fig. 6c). From visual inspection of the broken yarns, it seems that the epoxy penetrated better into the yarn due to its lower viscosity and smaller particles while the cement paste only covered a lesser depth but most of the core remained loose.

3.3 Stiffness of reinforcement and tension stiffening in the composite behaviour

The slopes of the load-deformation-curves in the hardening phase represent the stiffnesses of the textile reinforcement (E_{tc}), which were determined from linear regression and the mean of the two specimens per configuration (see green lines in Fig. 4 and Fig. 5). The directly knitted textile reinforcement displayed a much lower stiffness when compared to the notional material stiffness since most of the deformation is due to stretching (with concomitant lateral contraction) of the textile fabric as a whole rather than actual deformation of individual yarns. The interlocked double-layer knitting pattern exhibited a more flexible behaviour than the single layer fabrics (1-1 and 2-2) and the integration of ribs decreased stiffness even more.

The specimens with straight inlays showed much higher stiffness and the behaviour was dependent on the fibre material and the coating type. The aramid yarns with cement paste coating displayed a much lower stiffness when compared to the specimens with epoxy coating, which even exceeded the notional material stiffness from the material documentation (Table 1). The coated textile reinforcement acts as a composite (textile-coating) within a composite (reinforcement-concrete). Therefore, more investigations and separated tests on the rovings with and without coatings are currently carried out to assess the contribution of different components in the double-composite behaviour. The specimens with glass fibre rovings exhibited the same phenomenon whereas the carbon fibre inlays displayed a lower stiffness compared to the notional material stiffness.

In all specimens with a hardening phase, there was a distinct effect of tension stiffening. The interaction between reinforcement and concrete leads to a stress transfer between the two components and a shift of the load-deformation curve (Fig. 7). The Tension Chord Model [13], well established in conventionally reinforced concrete – assuming a constant bond shear stress as long as the reinforcement is elastic – can be adjusted to account for the different type of reinforcement and used for the assessment of the bond stresses following Eq. (2). The mean crack spacings in Eq. (2), and the crack widths used for validation, can be obtained by automated crack detection and measurement (ACDM) [14] using digital image correlation (DIC). These evaluations are currently in progress.

$$\tau_b = \frac{2 \cdot \Delta\varepsilon \cdot a_t \cdot E_{tc}}{s_r} \tag{2}$$

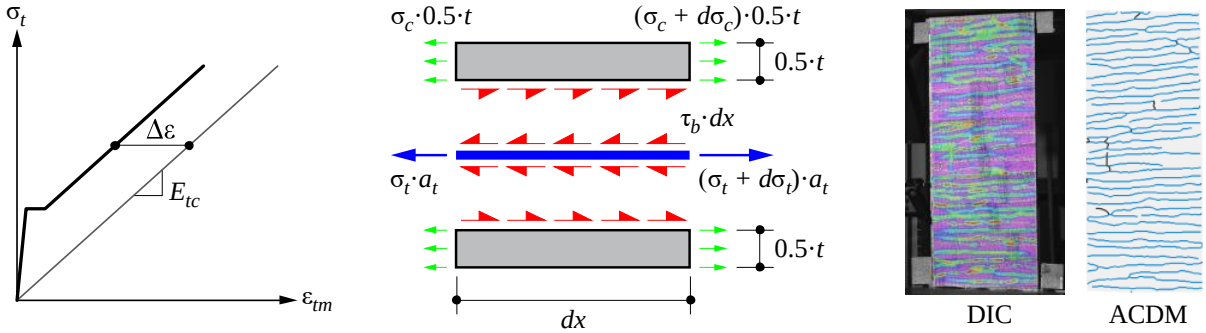

Fig. 7 Adapted tension chord model: (a) tension stiffening in stress-strain-relationship; (b) equilibrium of tensile and bond stresses; (c) crack detection using DIC and ACDM.

4 Conclusions

Results show that (i) in knitted textiles with high-strength fibrous materials, the ultimate strength of the rovings is significantly reduced due to the interlocked structure of the yarns and their vulnerability to lateral loading; (ii) the inclusion of straight rovings as inlays within the base fabric increases the utilisation of the fibres to an adequate level; (iii) glass and carbon fibres are considerably more brittle than

aramid and therefore, triggered by the concentrated deviation forces at the crack edges, fail shortly after crack formation when coated with cement paste; and (iv) the efficiency and stiffness can be highly improved by impregnating the fibres with epoxy instead. Regarding the behaviour of the textile-coating composite within the reinforcement-concrete composite, further research is required.

The load-deformation behaviour of the tension ties can be modelled using the tension chord model, which requires only few parameters and allows for the back-calculation of the bond stresses. This information can be used for the prediction of elements under different loading conditions such as bending or shear. A firm mechanical basis is needed to develop a consistent design model considering safety concepts for brittle materials and code compliance.

Acknowledgements

The authors gratefully acknowledge Dr. Mariana Popescu from Block Research Group (ETHZ) and Dr. Lex Reiter from the Chair of Physical Chemistry of Building Materials (ETHZ) for their technical and practical expertise as well as the students Seraina Buholzer and Salome Geiser for their valuable support during preparation and testing of the specimens shown in this paper. This research is supported by the National Centre for Competence in Research in Digital Fabrication, funded by the Swiss National Science Foundation (project number 51NF40-141853).

References

[1] A. Peled, B. Mobasher, and A. Bentur, *Textile reinforced concrete*. Boca Raton, FL: CRC Press, Taylor & Francis Group, 2017.

[2] T. Quadflieg, S. Leimbrink, T. Gries, and O. Stolyarov, 'Effect of coating type on the mechanical performance of warp-knitted fabrics and cement-based composites', *J. Compos. Mater.*, vol. 52, no. 19, pp. 2563–2576, Aug. 2018, doi: 10.1177/0021998317750003.

[3] J. Hegger, M. Horstmann, S. Voss, and N. Will, 'Textilbewehrter Beton: Tragverhalten, Bemessung und Anwendung', *Beton- Stahlbetonbau*, vol. 102, no. 6, pp. 362–370, Jun. 2007, doi: 10.1002/best.200700552.

[4] M. Fernàndez Ruiz and A. Muttoni, 'Building in a lighter and more sustainable manner: textile reinforced concrete for thin structural elements', cemsuisse, Schlussreport 201407, Dec. 2017.

[5] M. Popescu, M. Rippmann, T. Van Mele, and P. Block, 'Complex concrete casting: knitting stay-in-place formwork', in *Proceedings of the IASS 2016 Tokyo Symposium: Spatial Structures in the 21st Century*, Tokyo, Japan, 2016, p. 1278.

[6] M. Lee, J. Mata-Falcón, M. Popescu, P. Block, and W. Kaufmann, 'Potential approaches for reinforcing complex concrete structures with integrated flexible formwork', in *Proceedings for Digital Concrete 2020*, Eindhoven, Netherlands, Jul. 2020, vol. accepted for publication.

[7] M. Popescu, L. Reiter, A. Liew, T. Van Mele, R. J. Flatt, and P. Block, 'Building in Concrete with an Ultra-lightweight Knitted Stay-in-place Formwork: Prototype of a Concrete Shell Bridge', *Structures*, vol. 14, pp. 322–332, Jun. 2018, doi: 10.1016/j.istruc.2018.03.001.

[8] M. Popescu *et al.*, 'Structural design, digital fabrication and construction of the cable-net and knitted formwork of the KnitCandela concrete shell', *Structures*, p. S2352012420300655, Mar. 2020, doi: 10.1016/j.istruc.2020.02.013.

[9] 'DIN EN 196-1:2016-11, Prüfverfahren für Zement_- Teil_1: Bestimmung der Festigkeit; Deutsche Fassung EN_196-1:2016', Beuth Verlag GmbH. doi: 10.31030/2482416.

[10] International Federation for Structural Concrete, *fib model code for concrete structures 2010*. Berlin: Ernst & Sohn, 2013.

[11] RILEM Technical Committee 232-TDT (Wolfgang Brameshuber), 'Recommendation of RILEM TC 232-TDT: test methods and design of textile reinforced concrete', *Mater. Struct.*, vol. 49, no. 12, pp. 4923–4927, Dec. 2016, doi: 10.1617/s11527-016-0839-z.

[12] J. Yu, C. K. Leung, and V. C. Li, 'Why nominal cracking strength can be lower for later cracks in strain-hardening cementitious composites with multiple cracking?', in *Proceedings of the 10th International Conference on Fracture Mechanics of Concrete and Concrete Structures*, Jun. 2019, doi: 10.21012/FC10.234225.

[13] P. Marti, M. Alvarez, W. Kaufmann, and V. Sigrist, 'Tension chord model for structural concrete', *Struct. Eng. Int.*, vol. 8, no. 4, pp. 287–298, 1998.

[14] N. Gehri, J. Mata-Falcón, and W. Kaufmann, 'Automated Crack Detection and Measurement based on Digital Image Correlation', *Constr. Build. Mater.*, vol. submitted for publication, 2020.